Accepted Manuscript

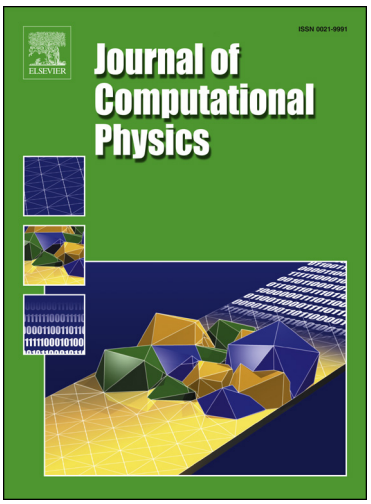

A RBF-based differential quadrature method for solving two-dimensional variable-order time fractional advection-diffusion equation

Jianming Liu, Xinkai Li, Xiuling Hu

PII: S0021-9991(19)30092-0
DOI: https://doi.org/10.1016/j.jcp.2018.12.043
Reference: YJCPH 8480

To appear in: *Journal of Computational Physics*

Received date: 22 June 2018
Revised date: 25 November 2018
Accepted date: 13 December 2018

Please cite this article in press as: J. Liu et al., A RBF-based differential quadrature method for solving two-dimensional variable-order time fractional advection-diffusion equation, *J. Comput. Phys.* (2019), https://doi.org/10.1016/j.jcp.2018.12.043

Highlights

- A new numerical technique is developed for a variable-order time fractional advection-diffusion equation with the Dirichlet and Neumann boundary conditions.
- The method is validated by the well documented test examples involving variable-order fractional modelling of air pollution.
- The numerical results demonstrate that the proposed method can provide accurate solutions.
- The current method can be extended to other types of variable-order fractional equations.

A RBF-based differential quadrature method for solving two-dimensional variable-order time fractional advection-diffusion equation

February 22, 2019

Jianming Liu[a] , Xinkai Li[b, 1] and Xiuling Hu[a]

[a] School of Mathematics and Statistics, Jiangsu Normal University, Xuzhou 221116, China
[b] Faculty of Technology, De Montfort University, Leicester LE1 9BH, England

Abstract

Numerical simulation technique of two-dimensional variable-order time fractional advection-diffusion equation is developed in this paper using radial basis function-based differential quadrature method (RBF-DQ). To the best of the authors' knowledge, this is the first application of this method to variable-order time fractional advection-diffusion equations. For the general case of irregular geometries, the meshless local form of RBF-DQ is used and the multiquadric type of radial basis functions is selected for the computations. This approach allows one to define a reconstruction of the local radial basis functions to treat accurately both the Dirichlet and Neumann boundary conditions on the irregular boundaries. The method is validated by the well documented test examples involving variable-order fractional modeling of air pollution. The numerical results demonstrate that the proposed method provides accurate solutions for two-dimensional variable-order time fractional advection-diffusion equations.

Keywords: Variable-order time fractional; Neumann boundary condition; RBF-DQ; Differential quadrature method; Radial basis function

1 Introduction

In the field of classical physics, basic physical variables can be defined by integer-order differential operations, and the physical evolution can be described by integer-order differential equations. These models based on integer-order calculus have gained tremendous successes in the science and engineering. However, the standard integer-order time derivative is defined by the local limit, which is not suitable for describing the historical dependence process, for example, anomalous (dispersive) transport in disordered semiconductors, non-Debye relaxation in solid dielectrics, penetration of light beam through a turbulent medium, transport of resonance radiation in plasma, etc [1]. The integral term in the definition of fractional time derivative fully reflects the historical dependence of the status development, and is a powerful mathematical tool for modeling memory processes. The

[1]Corresponding author. xkl@dmu.ac.uk

modeling problems in complex physics, mechanics, biology and engineering science are the main driving force to promote fractional calculus theories and their applications, and the popularity makes the fractional time derivative calculus becoming a hot topic in research [2, 3]. For example, anomalous diffusion is not only an important physical subject, but also a practical problem commonly involved in engineering. The diffusion behavior of the anomalous diffusion cannot be accurately described by the classical diffusion law, which is usually characterized by slow dissipation or rapid diffusion over time and spatial correlation in a long range. Fractional differential equations can exactly characterize such physical and mechanical processes. It is also worth pointing out that fractional calculus has been increasingly applied in the constitutive modeling of non-Newtonian fluids [1]. The main reason for this development is that a fractional calculus model could describe simply and elegantly the complex characteristics of viscoelastic materials. The theories and applications of fractional differential operators can be referred to the books [1, 4].

In this study, we focus on the numerical method for the time fractional advection-diffusion equation. The fractional advection-diffusion equation is one of the main research models for the anomalous solute diffusion and migration in complex medium [5]. In some complex media, with the change of the medium structure during the diffusion process, the diffusion behavior will also change correspondingly. Hence, the process cannot be expressed by the integer-order differential equations. The order of the diffusion equation needs to be changed with time or space, and then the variable-order fractional equations should be considered. Lorenzo and Hartley first suggested the concept of variable order (or variable structure) operators [6]. In the paper [7], the authors developed a variable-order differential equation of motion for a spherical particle sedimenting in a quiescent viscous liquid. The variable-order differential operators in anomalous diffusion modeling is presented in [8] and a comparative study of constant-order and variable-order fractional models in characterizing memory property of systems is presented in [9]. Their researches showed that the constant-order fractional derivative has advantages in characterizing the long memory of systems and the variable-order fractional derivative has advantages in presenting the variable memory of systems. Due to their complexity, the numerical solutions for them are highly necessary and important in practice [10]. Some of the recent numerical researches on the topic of variable-order can be found in [11–20]. The methods used in these papers including finite difference method [11–14, 16, 20] and spectral collocation method [15, 17–19], however, are limited in their applications with complex geometries. Although the finite difference methods are nowadays very effective and popular, they are limited in practical engineering applications with complex geometries. There are some research works on the finite element methods for constant-order fractional advection-diffusion equation (see [21–23] and their references). Dehghan et al developed a homotopy analysis method to solve nonlinear fractional partial differential equations [24]. For parallel algorithms and the accelerated convergence techniques, we can refer to the papers [25–27]. It should be noted that most of these papers only considered dealing with Dirichlet boundary conditions.

In order to treat the complex computational domains and reduce grid dependencies, meshless techniques have become very popular in recent years. Meshless methods are based on nodes without mesh elements. The construction of shape function is built on a series of discrete nodes. The connection between the field point and the node is no longer realized by the element, thus, this technique gets rid of the constraint of the grid element. It is not necessary to carry on a mesh reconstruction when it involves grid distortion and grid movement. Clearly, the meshless method shows a more obvious advantage in solving the fractional advection-diffusion equation. There are many kinds of meshless methods in the present, such as, Smooth particle hydrodynamics method

(SPH), Element-free Galerkin method (EFG), Meshless local Petrov-Galerkin method (MLPG), Radial bases function method (RBF), Finite point method (FPM), Moving least square method (MLS), and so on [28]. The main difference is the use of different trial functions or equivalent forms of differential equations. There are some researches on meshless method for the numerical simulations of time fractional advection-diffusion equation. In the paper [29], the authors developed the method of approximate particular solutions (MAPS) for constant- and variable-order fractional diffusion models on Dirichlet or Neumann boundary conditions, which is defined in terms of a linear combination of the particular solutions of the inhomogeneous governing equations with traditional RBFs as the source term. But the final basis functions are very complicated and they only considered the rectangular domain. Dehghan and Abbaszadeh presented an EFG approach based on the reproducing kernel particle method for solving 2D fractional Tricomi-type equation with Robin boundary condition in [30]. MLS method is presented to solve the constant-order time fractional advection-diffusion equation in the paper [31,32]. For the variable-order time fractional advection-diffusion equation, we can refer to the paper [10]. The MLS method consists of a local weighted least square fitting, valid on a small neighborhood of a point and only based on the information provided by its N closest points. However, the shape function in MLS method is not satisfied with Kronecker δ function character and the boundary condition can not be directly enforced, which increase the difficulty for the treatment of boundary conditions. It should be noted that the above most of works are on the problem with Dirichlet boundary conditions.

RBF method is a real meshless method for solving partial differential equations, and it has nothing to do with the spatial dimension [33,34]. Radial basis function-based differential quadrature method (RBF-DQ) is a meshless method which has originated from the concept of differential quadrature. Classical differential quadrature (DQ) method began from the idea of conventional integral quadrature [35], but, it cannot directly be applied to problems with irregular geometries. In order to treat any geometries, a meshfree local RBF-DQ approach to solve the two-dimensional incompressible Navier-Stokes equations is developed in [36]. Due to the vast flexibility, RBF-DQ method has been successfully used to study many scientific and engineering problems [34, 37–44]. The aim of our study is to improve upon the current numerical methods and adopt RBF-DQ method to study the variable-order time fractional advection-diffusion equations with not only the Dirichlet boundary conditions but also the Neumann boundary conditions. To the best of the authors' knowledge, the corresponding research is very limited.

The paper is organized as follows. Section 2 formulates the mathematical model being considered as a time fractional advection-diffusion equation in this paper. In Section 3, the time discretization technique used for the variable-order time fractional advection-diffusion equation is presented. RBF-based differential quadrature methods over the general geometry with Dirichlet and Neumann boundary conditions are shown in Section 4. In Section 5, computational results are presented based on two dimension benchmark problems with complex geometries. The numerical results demonstrate the efficiency and versatility of the proposed approach. Finally, some concluding remarks are given in Section 6.

2 Time fractional advection-diffusion model

A general two-dimensional convection-diffusion equation applying fractional derivatives has been developed in [10]. The complete equation for the variable-order time fractional advection-diffusion

equation is

$$ {}_0^cD_t^{\alpha(\mathbf{x},t)}u(\mathbf{x},t) = \kappa(\mathbf{x},t)\Delta u(\mathbf{x},t) - \mathbf{v}(\mathbf{x},t)\cdot\nabla u(\mathbf{x},t) + f(\mathbf{x},t), \quad \mathbf{x}=(x,y)\in\Omega\subset\mathbb{R}^2, \quad t>0, \tag{1} $$

subject to the following general initial and boundary conditions

$$ \begin{aligned} &u(\mathbf{x},0) = \phi(\mathbf{x}), \quad \mathbf{x}\in\Omega, \\ &\mathbb{B}u(\mathbf{x},t) = \psi(\mathbf{x},t), \quad \mathbf{x}\in\partial\Omega, \quad t>0, \end{aligned} \tag{2} $$

where $\Delta u = \frac{\partial^2 u}{\partial x^2} + \frac{\partial^2 u}{\partial y^2}$, $\nabla u = (\frac{\partial u}{\partial x}, \frac{\partial u}{\partial y})$, and $\mathbb{B}$ denotes the operator with Dirichlet or Neumann boundary conditions. Ω is a bounded domain in $\mathbb{R}^2$, $\partial\Omega$ is the boundary of Ω, $\kappa(\mathbf{x},t) > 0$ is the diffusion coefficient function, $\mathbf{v}$(x,t) is advection velocity, and $f(\mathbf{x},t)$, $\phi(\mathbf{x})$, $\psi(\mathbf{x},t)$ are given functions, respectively. Dirichlet boundary condition fixes the value for the solution at the edge of the domain, while Neumann boundary condition means to impose the flux through that domain boundary. In the paper [10], the authors gave a meshless method by MLS to study the present model with Dirichlet boundary condition. However, for the processes of transport and diffusion of pollutants in the atmosphere, the Neumann boundary condition should be more suitable.

In Equation (1), ${}_0^cD_t^{\alpha(\mathbf{x},t)}u(\mathbf{x},t)$ denotes the variable-order time fractional derivative operator in the Caputo sense defined by

$$ {}_0^cD_t^{\alpha(\mathbf{x},t)}u(\mathbf{x},t) = \begin{cases} \frac{1}{\Gamma(1-\alpha(\mathbf{x},t))}\int_0^t \frac{1}{(t-\xi)^{\alpha(\mathbf{x},t)}}\frac{\partial u(\mathbf{x},\xi)}{\partial\xi}d\xi, & 0<\alpha(\mathbf{x},t)<1, \\ \frac{\partial u(\mathbf{x},t)}{\partial t}, & \alpha(\mathbf{x},t)=1. \end{cases} \tag{3} $$

where Γ is the gamma function.

3 The time discretization approximation

In this study, we focus on the RBF-DQ method for the variable-order time fractional advection-diffusion equation on complex geometries with different boundary conditions. We first present the time discretization approximation for the variable-order time fractional derivative. Following the time discretization method proposed in the papers [10, 31, 45], the variable-order time fractional operator ${}_0^cD_t^{\alpha(\mathbf{x},t)}u(\mathbf{x},t)$ takes the discrete form

$$ \begin{aligned} {}_0^cD_t^{\alpha(\mathbf{x},t)}u(\mathbf{x},t_{k+1}) &= \frac{1}{\Gamma(1-\alpha(\mathbf{x},t_{k+1}))}\sum_{j=0}^{k}\int_{t_j}^{t_{j+1}}\frac{1}{(t_{k+1}-\xi)^{\alpha(\mathbf{x},t_{k+1})}}\frac{\partial u(\mathbf{x},\xi)}{\partial\xi}d\xi, \\ &= \frac{1}{\Gamma(1-\alpha(\mathbf{x},t_{k+1}))}\sum_{j=0}^{k}\frac{u(\mathbf{x},t_{j+1})-u(\mathbf{x},t_j)}{\Delta t}\int_{t_j}^{t_{j+1}}\frac{1}{(t_{k+1}-\xi)^{\alpha(\mathbf{x},t_{k+1})}}d\xi + R_{k+1}, \\ &= \frac{\Delta t^{-\alpha(\mathbf{x},t_{k+1})}}{\Gamma(2-\alpha(\mathbf{x},t_{k+1}))}\sum_{j=0}^{k} b_{k-j}(\mathbf{x},t_{k+1})(u(\mathbf{x},t_{j+1})-u(\mathbf{x},t_j)) + R_{k+1} \\ &= \frac{\Delta t^{-\alpha(\mathbf{x},t_{k+1})}}{\Gamma(2-\alpha(\mathbf{x},t_{k+1}))}\sum_{j=0}^{k} b_j(\mathbf{x},t_{k+1})(u(\mathbf{x},t_{k-j+1})-u(\mathbf{x},t_{k-j})) + R_{k+1} \end{aligned} \tag{4} $$

where $t_k = k\Delta t$ for $k = 0, 1, \ldots, M$ and $M = T/\Delta t$, and $b_j(\mathbf{x},t_{k+1}) = (j+1)^{1-\alpha(\mathbf{x},t_{k+1})} - j^{1-\alpha(\mathbf{x},t_{k+1})}$. The truncation error R_{k+1} is subjected to

$$ |R_{k+1}| \le C\Delta t^{2-\alpha(\mathbf{x},t_{k+1})}. \tag{5} $$

Substituting Equation (4) into Equation (1), and with the θ-weighted scheme ($\theta \in [0,1]$), we can obtain

$$\begin{aligned} & u(\mathbf{x},t_{k+1}) - \theta\mu(\mathbf{x},t_{k+1})\left[\kappa(\mathbf{x},t_{k+1})\Delta u(\mathbf{x},t_{k+1}) - \mathbf{v}(\mathbf{x},t_{k+1})\cdot\nabla u(\mathbf{x},t_{k+1})\right] \\ & \quad = u(\mathbf{x},t_k) + (1-\theta)\mu(\mathbf{x},t_{k+1})\left[\kappa(\mathbf{x},t_{k+1})\Delta u(\mathbf{x},t_k) - \mathbf{v}(\mathbf{x},t_{k+1})\cdot\nabla u(\mathbf{x},t_k)\right] \\ & \quad - \sum_{j=1}^{k} b_j(\mathbf{x},t_{k+1})(u(\mathbf{x},t_{k-j+1}) - u(\mathbf{x},t_{k-j})) + \mu(\mathbf{x},t_{k+1})f(\mathbf{x},t_{k+1}) + \overline{R}_{k+1} + \overline{M}_{k+1}, \end{aligned} \tag{6}$$

where

$$\mu(\mathbf{x},t_{k+1}) = \Delta t^{\alpha(\mathbf{x},t_{k+1})}\Gamma(2-\alpha(\mathbf{x},t_{k+1})), \tag{7}$$

and

$$|\overline{R}_{k+1}| \le \overline{C}\Delta t^2, \quad |\overline{M}_{k+1}| \le \overline{C}_1(1-\theta)\Delta t^{1+\alpha(\mathbf{x},t_{k+1})}. \tag{8}$$

Using the notations $u^k = u^k(\mathbf{x})$ as the numerical approximation to $u(\mathbf{x},t_k)$, $\mu^k = \mu(\mathbf{x},t_k)$, $\kappa^k = \kappa(\mathbf{x},t_k)$, $\mathbf{v}^k = \mathbf{v}(\mathbf{x},t_k) = (v_1(\mathbf{x},t_k), v_2(\mathbf{x},t_k))$, $b_j^k = b_j(\mathbf{x},t_k)$ and $f^k = f(\mathbf{x},t_k)$, respectively, then Equation (1) can be discretized as follows

$$\begin{aligned} & u^{k+1} - \theta\mu^{k+1}\left[\kappa^{k+1}\Delta u^{k+1} - \mathbf{v}^{k+1}\cdot\nabla u^{k+1}\right] \\ & \quad = u^k + (1-\theta)\mu^{k+1}\left[\kappa^{k+1}\Delta u^k - \mathbf{v}^{k+1}\cdot\nabla u^k\right] - \sum_{j=1}^{k} b_j^{k+1}(u^{k-j+1} - u^{k-j}) + \mu^{k+1}f^{k+1}. \end{aligned} \tag{9}$$

For $\theta = 1$, Equation (9) is the same as the scheme proposed by the paper [31] for constant-order time fractional advection-diffusion equation. The equation (9) can be rearranged as

$$\begin{aligned} & u^{k+1} - \theta\mu^{k+1}\left[\kappa^{k+1}\Delta u^{k+1} - \mathbf{v}^{k+1}\cdot\nabla u^{k+1}\right] \\ & \quad = (1-b_1^{k+1})u^k + (1-\theta)\mu^{k+1}\left[\kappa^{k+1}\Delta u^k - \mathbf{v}^{k+1}\cdot\nabla u^k\right] \\ & \qquad + \sum_{j=1}^{k-1}(b_j^{k+1} - b_{j+1}^{k+1})u^{k-j} + b_k^{k+1}u^0 + \mu^{k+1}f^{k+1}. \end{aligned} \tag{10}$$

4 RBF-based differential quadrature method

4.1 Basic RBF-based differential quadrature method

The idea of differential quadrature method came from the numerical differentiation, that any derivative at a node can be approximated by a linear weighted sum of all the functional values on a line. In differential quadrature method, as the numerical differentiation, the derivative values $u^{(m)}(\mathbf{x})$ at the centre $\mathbf{x}_i$ are approximated by a linear weighted sum of the function values at a set of nodes in a closed domain defined as

$$u_x^{(m)}(\mathbf{x_i}) \approx \sum_{j=1}^{N} w_{ij}^{(m)} u(\mathbf{x}_j), \quad u_y^{(m)}(\mathbf{x_i}) \approx \sum_{j=1}^{N} \overline{w}_{ij}^{(m)} u(\mathbf{x}_j), \tag{11}$$

for $i = 1, \cdots, N$, where $w_{ij}^{(m)}$ and $\overline{w}_{ij}^{(m)}$ are the weighting coefficients for derivatives of order m with respect to x and y, respectively. In RBF-DQ method [36,46], the weighting coefficients of $w_{ij}^{(m)}$ and $\overline{w}_{ij}^{(m)}$ are specially determined by all the base functions as the test functions in Equation (11).

It should be noted that there are many choices of the basis functions in the RBF methods. In this study, due to the better performance for the interpolation of 2D scattered data [36,46,47], the

multiquadrics (MQ) basis function is used as the test function. The function in the region of Ω can be locally approximated by RBF-MQ as

$$h(x,y)=\sum_{j=1}^{N}\lambda_j\sqrt{(x-x_j)^2+(y-y_j)^2+c_j^2}+\lambda_{N+1}, \tag{12}$$

with shape parameter c_j. In order to make the problem be well-posed, the equation

$$\sum_{j=1}^{N}\lambda_j=0, \tag{13}$$

is enforced. Substituting Equation (13) into Equation (12) gives

$$h(x,y)=\sum_{j=1,j\neq i}^{N}\lambda_j g_j(x,y)+\lambda_{N+1}, \tag{14}$$

where

$$g_j(x,y)=\sqrt{(x-x_j)^2+(y-y_j)^2+c_j^2}-\sqrt{(x-x_i)^2+(y-y_i)^2+c_i^2}. \tag{15}$$

The number of unknowns in Equation (14) is N. As the setting in the paper [36], λ_{N+1} can be replaced by λ_i, and Equation (14) can be written as

$$h(x,y)=\sum_{j=1,j\neq i}^{N}\lambda_j g_j(x,y)+\lambda_i. \tag{16}$$

where $g_i(x,y)=1$ and $g_j(x,y)$, $(j=1,\cdots,N$, but $j\neq i)$ given by Equation (15) are a base vector for the function space of $h(x,y)$.

In RBF-DQ method, the weighting coefficients of $w_{ij}^{(m)}$, and $\overline{w}_{ij}^{(m)}$ are determined by all the base functions as the test function in Equation (11), and this gives

$$\sum_{k=1}^{N}w_{ik}^{(m)}=0, \tag{17a}$$

$$\frac{\partial^m g_j(x_i,y_i)}{\partial x^m}=\sum_{k=1}^{N}w_{ik}^{(m)}g_j(x_k,y_k),\ j=1,2,\cdots,N,\ \text{but}\ j\neq i. \tag{17b}$$

A linear system of N equations can be formed from equation (17) with N unknowns for the given i, and then the weighting coefficients $w_{ik}^{(m)}$ can be solved by a numerical method. In a similar manner, the weighting coefficients $\overline{w}_{ij}^{(m)}$ of the y-derivatives can also be computed by Equation (17) with x substituted by y.

Substitution of Equation (11) into time discretized equation (10) at an internal point $\mathbf{x_i} = (x_i, y_i)$, with u_i^{k+1} as the approximation solution of $u(\mathbf{x}_i, t_{k+1})$, yields

$$\begin{aligned} u_i^{k+1} - \theta\mu_i^{k+1}\left[\kappa_i^{k+1}\sum_{j=1}^{N}\left(w_{ij}^{(2)}+\overline{w}_{ij}^{(2)}\right)u_j^{k+1} - \sum_{j=1}^{N}\left(w_{ij}^{(1)}v_{1,i}^{k+1}+\overline{w}_{ij}^{(1)}v_{2,i}^{k+1}\right)u_j^{k+1}\right] \\ = (1-b_{i,1}^{k+1})u_i^k + (1-\theta)\mu_i^{k+1}\left[\kappa_i^{k+1}\sum_{j=1}^{N}\left(w_{ij}^{(2)}+\overline{w}_{ij}^{(2)}\right)u_j^{k} - \sum_{j=1}^{N}\left(w_{ij}^{(1)}v_{1,i}^{k+1}+\overline{w}_{ij}^{(1)}v_{2,i}^{k+1}\right)u_j^{k}\right] \\ + \sum_{j=1}^{k-1}(b_{i,j}^{k+1}-b_{i,j+1}^{k+1})u_i^{k-j} + b_{i,k}^{k+1}u_i^0 + \mu_i^{k+1}f_i^{k+1}, \end{aligned} \tag{18}$$

where

$$\mu_i^{k+1} = \mu(\mathbf{x}_i, t_{k+1}), \quad v_{1,i}^{k+1} = v_1(\mathbf{x}_i, t_{k+1}), \quad v_{2,i}^{k+1} = v_2(\mathbf{x}_i, t_{k+1}),$$
$$\kappa_i^{k+1} = \kappa(\mathbf{x}_i, t_{k+1}), \quad b_{i,j}^{k+1} = b_j(\mathbf{x}_i, t_{k+1}), \quad f_i^{k+1} = f(\mathbf{x}_i, t_{k+1}).$$

4.2 Local RBF-based differential quadrature method

When the number of the nodal points, N, is large, the coefficient matrix of Equation (17) may be ill-conditioned. This limits its application. Hence, we mainly use the local RBF-DQ method to solve the variable-order time fractional advection-diffusion equation.

The key of local RBF-based differential quadrature method is that the m-order derivatives of $u(\mathbf{x})$ at $\mathbf{x}_i$ are approximated by the function values at a set of nodes in the neighborhood of $\mathbf{x}_i$ with N_i nodes (including $\mathbf{x}_i$). That is

$$u_x^{(m)}(\mathbf{x_i}) \approx \sum_{j=1}^{N_i} w_{ij}^{(m)}u(\mathbf{x}_j), \quad u_y^{(m)}(\mathbf{x_i}) \approx \sum_{j=1}^{N_i} \overline{w}_{ij}^{(m)}u(\mathbf{x}_j), \quad i = 1, 2, \cdots, N. \tag{20}$$

The corresponding coefficients $w_{ij}^{(m)}$ and $\overline{w}_{ij}^{(m)}$ are determined by Equation (17) with N_i local support nodes in the neighbor of $\mathbf{x}_i$.

Substitution of Equation (20) into time discretized equation (10) at an internal point $\mathbf{x_i}$, by the local RBF-based differential quadrature method, yields

$$\begin{aligned} u_i^{k+1} - \theta\mu_i^{k+1}\left[\kappa_i^{k+1}\sum_{j=1}^{N_i}\left(w_{ij}^{(2)}+\overline{w}_{ij}^{(2)}\right)u_j^{k+1} - \sum_{j=1}^{N_i}\left(w_{ij}^{(1)}v_{1,i}^{k+1}+\overline{w}_{ij}^{(1)}v_{2,i}^{k+1}\right)u_j^{k+1}\right] \\ = (1-b_{i,1}^{k+1})u_i^k + (1-\theta)\mu_i^{k+1}\left[\kappa_i^{k+1}\sum_{j=1}^{N_i}\left(w_{ij}^{(2)}+\overline{w}_{ij}^{(2)}\right)u_j^{k} - \sum_{j=1}^{N_i}\left(w_{ij}^{(1)}v_{1,i}^{k+1}+\overline{w}_{ij}^{(1)}v_{2,i}^{k+1}\right)u_j^{k}\right] \\ + \sum_{j=1}^{k-1}(b_{i,j}^{k+1}-b_{i,j+1}^{k+1})u_i^{k-j} + b_{i,k}^{k+1}u_i^0 + \mu_i^{k+1}f_i^{k+1}. \end{aligned} \tag{21}$$

As shown in the previous subsection, the RBF-DQ approximation of the function contains a shape parameter c that could be dependent on the nodes and must be pre-determined by the user. Actually, choosing the parameter c is still an open problem for representing radial basis function that has received the attention of many researchers. For technical details of determining the optimal value of c, the reader is directed to references [36, 41, 48]. In this study, we use the method

of normalization of supporting region suggested in the paper of [36]. This method transforms the local support points to a unit circle in two-dimensional problem and the discussion about the optimal shape parameter is confined to the MQ test function in the unit circle. The coordinate transformation is

$$\bar{x} = \frac{x}{D_i},\ \bar{y} = \frac{y}{D_i}, \tag{22}$$

where D_i is the diameter of the minimal circle including all supporting points for the computational node i. Then, the corresponding MQ test function in Equation (12) becomes

$$\sqrt{\left(\bar{x} - \frac{x_j}{D_i}\right)^2 + \left(\bar{y} - \frac{y_j}{D_i}\right)^2 + c^2},\ j = 1, \ldots, N_i.$$

The coordinate transformation (22) also changes the formulas of the weighting coefficients in Equation (17). The optimal value of shape parameter c depends on the number of local supporting points. If there are no special instructions, for the sake of consistency, $c^2 = 15$ is used in all numerical examples in the paper. Furthermore, the number of the supporting points has an important impact on the numerical accuracy. In order to obtain the nodal connectivity, in present study, we use triangulation to obtain the nodal connectivity and take the nearest neighbor points in two layers as the supporting grids [49].

4.3 Boundary treatment

The boundary treatment for Dirichlet boundary condition in collocation method is trivial, but the special treatment should be designed for the derivative boundary conditions. In the following, we present how to construct system equations for problems, respectively, with the different boundary conditions respectively.

Suppose $\mathbf{U}$ is the vector that collects all nodal values, i.e.

$$\mathbf{U}^T_{N\times 1} = [u_1^{k+1}, u_2^{k+1}, \cdots, u_{N-1}^{k+1}, u_N^{k+1}]. \tag{23}$$

Using the present local RBF-DQ method, for the problem with only Dirichlet boundaries, at an internal node $\mathbf{x}_i$, the discretized governing equations can be obtained by Equation (21). For any boundary nodal point $\mathbf{x}_I^b$, the equation

$$u_I^{k+1} = \psi(\mathbf{x}_I^b, t_{k+1}), \tag{24}$$

is enforced. Then the system equations are integrated by Equation (21) at all internal nodal points and Equation (24) at all Dirichlet boundary points. The final system of equations can be given as

$$\mathbf{K}_{N\times N}\mathbf{U}_{N\times 1} = \mathbf{F}_{N\times 1}, \tag{25}$$

where the global system matrix $\mathbf{K}_{N\times N}$ is formed by the left-hand terms of Equations (21) and (24), and the global vector $\mathbf{F}_{N\times 1}$ expresses the right-hand terms of Equations (21) and (24). For local RBF-DQ method, the coefficient matrix K is sparse, and the bandwidth is the number of local supporting points. The sparse system can be solved by any direct method.

For the Neumann boundary condition, in the paper [36], one-sided second order finite difference scheme was used to deal with Neumann boundary conditions, in which two different approaches were used to discretize the governing equations and the boundary conditions. In our study, for the

variable-order time fractional advection-diffusion equation, we can still apply the local RBF-DQ method of (20) to the Neumann boundary condition, which can be formulated as

$$\frac{\partial u(x_I^b, y_I^b)}{\partial \mathbf{n}} \approx \sum_{j=1}^{N_I} (w_{Ij}^{(1)} n_x + \overline{w}_{Ij}^{(1)} n_y) u_j, \tag{26}$$

at a Neumann boundary nodal $\mathbf{x}_I^b$. Hence, for any Neumann boundary nodal $\mathbf{x}_I^b$, the equation

$$\sum_{j=1}^{N_I} (w_{Ij}^{(1)} n_x + \overline{w}_{Ij}^{(1)} n_y) u_j = \psi(\mathbf{x}_I^b, t_{k+1}), \tag{27}$$

is formed. The final system of equations (25) can be integrated by Equations (21) at all internal nodal points and Equations (27) on the Neumann boundary nodal points, clearly, the final matrix is still a sparse matrix.

5 Numerical examples

In this section, numerical experiments, demonstrating the accuracy and the effectiveness of the RBF-DQ method for variable-order time fractional advection-diffusion equation with the Dirichlet or the Neumann boundary conditions, are presented. Two different test examples with known analytical solutions are considered. In each case, comparisons between the corresponding analytical solutions or numerical solutions are presented. It should be noted that these test examples were used with the Dirichlet boundary conditions only in [10], however, it has been extended to both the Dirichlet and the Neumann conditions on different solution domains for the RBF-DQ method developed in this paper. The Gauss pulse solution is also considered. Furthermore, a practical problem is also studied based on a variable-order fractional air pollution model. For the numerical simulations, if there are no special instructions, the parameter $\theta = 1$ in Equation (21) is used in all numerical calculations, although it is valid for any value of $\theta \in [0, 1]$. Clearly, for this special value, Equation (21) becomes a well-known implicit scheme. And if there are no special instructions, the time step Δt is 1/200. All the numerical tests are carried on a personal Macbook Pro laptop (macOS Mojave 10.14, 2.2 GHZ Intel Core i7, 16GB 1600 MHz DDR3) with Matlab R2015b.

In order to demonstrate the accuracy of the proposed method, the L^2, L^∞ errors and Root-Mean-Square (RMS) of errors are measured using the following definitions:

$$L^2 = \sqrt{\sum_{i=1}^{N} |u(\mathbf{x}_i) - u^h(\mathbf{x}_i)|^2 \Big/ \sum_{i=1}^{N} |u(\mathbf{x}_i)|^2},$$

$$L^\infty = \max_{1 \le i \le N} \left| u(\mathbf{x}_i) - u^h(\mathbf{x}_i) \right|, \ \text{RMS} = \sqrt{\frac{1}{N} \left(\sum_{i=1}^{N} |u(\mathbf{x}_i) - u^h(\mathbf{x}_i)|^2 \right)},$$

where $u^h(\mathbf{x}_i)$ is the numerical solution of $u(\mathbf{x}_i)$ and N is the total number of nodal points.

5.1 Test problem with Dirichlet boundary condition

In this subsection, we look for a numerical solution of the variable-order time fractional advection-diffusion equation

$$\frac{\partial^{\alpha(\mathbf{x},t)}u(\mathbf{x},t)}{\partial t^{\alpha(\mathbf{x},t)}} = \frac{\partial^2 u(\mathbf{x},t)}{\partial x^2} + \frac{\partial^2 u(\mathbf{x},t)}{\partial y^2} - \frac{\partial u(\mathbf{x},t)}{\partial x} - \frac{\partial u(\mathbf{x},t)}{\partial y} + \frac{2t^{2-\alpha(\mathbf{x},t)}}{\Gamma(3-\alpha(\mathbf{x},t))} + 2x + 2y - 4, \quad (28)$$

satisfying an initial and the Dirichlet boundary conditions of Equation (2) on the domain Ω. The rectangular domain $\Omega = [0,1] \times [0,1]$ and the unit circular domain are firstly considered for the current numerical simulations. Therefore, the initial and boundary conditions corresponding to Equation (2) can be calculated from an exact solution $u(\mathbf{x},t) = x^2 + y^2 + t^2$, which was used as an example in the paper [10]. The point distribution for the rectangular and circular domains are

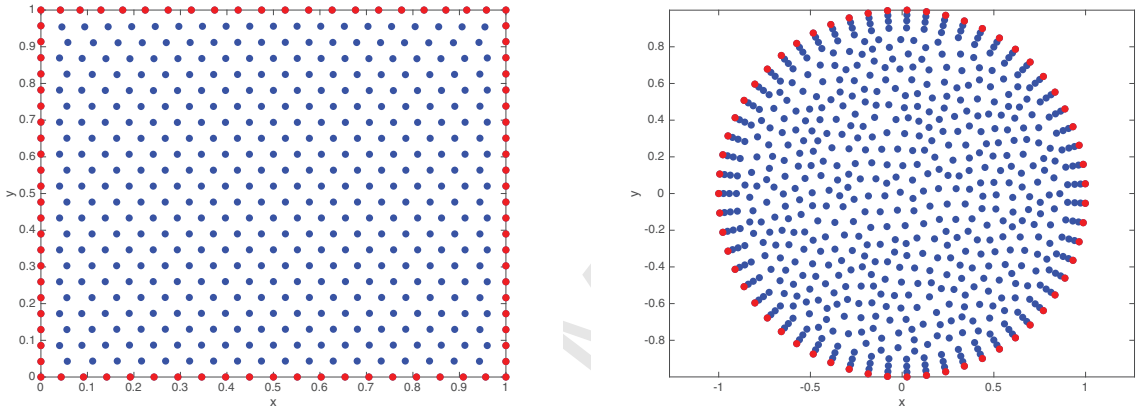

(a) The rectangular domain. (b) The circular domain.

Figure 1: Point distribution of the rectangular domain ($N = 494$) and circular domain ($N = 646$).

shown in Fig. 1. The total numbers of point distribution are 494 and 646 for the rectangular domain and the circular domain, respectively.

As a test of RBF-DQ method, we solve Equation (28) with $\Delta t = 1/200$ for the Dirichlet boundary condition. The approximate solutions at time $t = 1$ for $\alpha(\mathbf{x},t) = 0.8 - 0.1\cos(xt)\sin(x) - 0.1\cos(yt)\sin(y)$ and the absolute errors are demonstrated in Fig. 2 for the rectangular domain and in Fig. 3 for the circular domain. It is clearly seen that the approximate solutions obtained by the current local RBF-DQ method are in good agreement with the exact solutions for the regular and the irregular domains. Hence, it can be concluded that the current local RBF-DQ method can provide numerical solutions with good accuracy to the variable-order time fractional advection-diffusion problems.

In order to quantify the accuracy of the RBF-DQ method, the L^2, L^∞ and RMS errors at time $t = 1$ for two constant orders $\alpha = 0.5,\ 0.8$ and one variable order $\alpha(\mathbf{x},t) = 0.8 - 0.1\cos(xt)\sin(x) - 0.1\cos(yt)\sin(y)$ are shown in Table 1. It can be seen that the results from the local RBF-DQ method presented in this paper have very good accuracy on both constant and variable order time fractional advection-diffusion equations.

A comparison of the errors, such as L^∞ and RMS errors, between our solutions and Tayebi's MLS' solutions, is shown in Table 2. Here we use the same uniform point distribution with 121

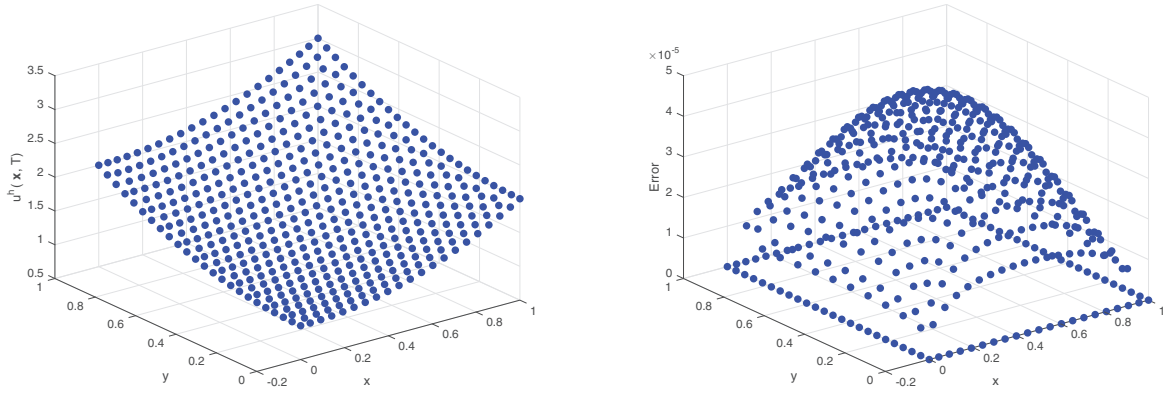

(a) The approximate solution.

(b) The absolute error.

Figure 2: The space graphs of the approximate solution and absolute error for Equation (28) with Dirichlet boundary condition on the rectangular domain ($N = 494$).

Table 1: L^2/L^∞ errors and RMS of errors obtained by local RBF-DQ method on different domains with Dirichlet boundary condition.

	Rectangular domain			Circular domain		
α	L^2	L^∞	RMS	L^2	L^∞	RMS
0.5	2.2570e-06	9.6598e-06	3.9326e-06	3.1875e-06	1.2322e-05	5.1341e-06
0.8	2.6859e-05	8.5059e-05	4.6797e-05	8.2842e-05	2.5405e-04	1.3343e-04
$\alpha(\mathbf{x}, t)$	1.5227e-05	4.5832e-05	2.6530e-05	9.2144e-05	2.8199e-04	1.4841e-04

points to simulate Equation (28) with the Dirichlet boundary condition on the rectangular domain $\Omega = [0, 1] \times [0, 1]$. The results reported in Table 2 show that the numerical errors achieved by the present method in some cases are slightly smaller than that obtained by the MLS method [10], in particular, for the variable order $\alpha(\mathbf{x}, t)$. This indicates that the current solutions, at least, are as good as the solutions obtained by MLS method [10]. This again reinforces our conclusion given earlier.

In order to explore the grid convergence, we choose three different grids and solve the same equations with the variable order $\alpha(\mathbf{x}, t)$ on the unit circular domain. To reduce the influence of time discretization error, we take a smaller time step $\Delta t = 1/1000$. The numerical results of L^2, L^∞ and RMS errors are shown in Table 3. It is found that the errors decrease as the number of grids increases. The condition numbers of the matrices for different grids are also reported. For the analysis of the convergence, the different θ in Equation (21) are also shown in Table 3. The results show there is no significant difference between $\theta = 1$ and $\theta = 1/2$.

Time convergence can be obtained by a fixed grid with different time steps. For this special test, we use the grid in Table 3 with $N = 873$ points on the unit circular domain. The different errors are presented in Table 4. Clearly, it shows that the errors decrease with time step sizes.

Table 2: Comparison of L^∞ errors and RMS of errors on the rectangular domain with Dirichlet boundary condition.

	MLS method in [10]		Present local RBF-DQ method	
α	L^∞	RMS	L^∞	RMS
0.5	3.2296e-05	1.6596e-05	4.1163e-05	3.1388e-05
0.8	2.1712e-04	1.1143e-04	1.2445e-04	7.2997e-05
$\alpha(\mathbf{x}, t)$	1.3394e-04	6.9272e-05	8.5857e-05	5.3835e-05

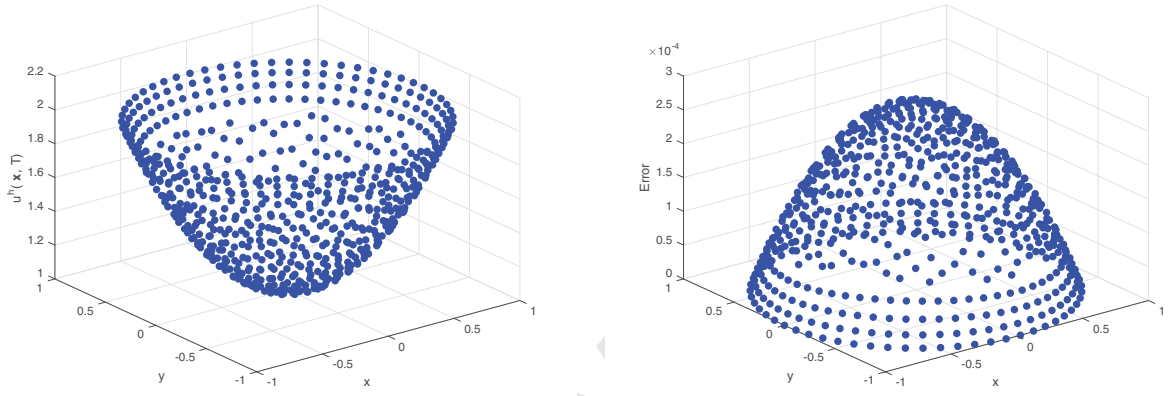

(a) The approximate solution.

(b) The absolute error.

Figure 3: The space graphs of the approximate solution and absolute error for Equation (28) with Dirichlet boundary condition on the unit circular domain ($N = 646$).

Furthemore, if we assume

$$\|\text{error}\|_{L^2} \approx C(\Delta t)^p,$$

then we can verify

$$-\log \|\text{error}\|_{L^2} \approx -\log C - p \log \Delta t.$$

Using the data in Table 4, we can obtain a linear fitting function

$$-\log \|\text{error}\|_{L^2} \approx 2.0848 - 1.3621 \log \Delta t.$$

So, for $\alpha(\mathbf{x}, t) = 0.8 - 0.1\cos(xt)\sin(x) - 0.1\cos(yt)\sin(y)$, the time discretization order is about 1.36, which is consistent with the theory of Equation (5). In the same table, the condition numbers of the matrices with different time steps are also reported. With the decrease of time step, the condition numbers are reduced. Clearly, CPU time costs are also increased as shown in Table 4. However, these quantities are within reasonable limits.

The accuracy of numerical results is also studied with changing the shape parameter c and the number of the supporting points. In the paper [36], Shu et al found that when the shape parameter c is fixed, with increase of the number of the supporting points, the approximate accuracy is improved. And with the increase of shape parameter c, the numerical accuracy is also improved. Fig. 4 shows

Table 3: Grid convergence of local RBF-DQ method with Dirichlet boundary condition ($\Delta t = 1/1000$).

	$\theta = 1.0$				$\theta = 0.5$			
N	L^2	L^∞	RMS	Cond.	L^2	L^∞	RMS	Cond.
214	2.8472e-05	1.1385e-04	4.4952e-05	5.618	2.8473e-05	1.1385e-04	4.4954e-05	3.227
421	7.4835e-06	2.7374e-05	1.1712e-05	9.584	7.4832e-06	2.7373e-05	1.1711e-05	5.177
873	2.9932e-06	1.0359e-05	4.7151e-06	35.88	2.9929e-06	1.0358e-05	4.7145e-06	17.25

Table 4: Time convergence of local RBF-DQ method with Dirichlet boundary condition ($N = 873$).

	$\theta = 1.0$					$\theta = 0.5$				
Δt	L^2	L^∞	RMS	Cond.	Sec.	L^2	L^∞	RMS	Cond.	Sec.
1/50	5.7446e-04	1.6355e-03	9.0490e-04	389.7	18.41	5.7498e-04	1.6371e-03	9.0573e-04	173.4	18.23
1/100	2.4377e-04	6.9665e-04	3.8399e-04	216.8	46.85	2.4387e-04	6.9696e-04	3.8415e-04	99.51	46.89
1/200	9.7826e-05	2.8113e-04	1.5410e-04	125.0	134.7	9.7843e-05	2.8118e-04	1.5413e-04	57.96	134.6
1/400	3.3469e-05	9.8944e-05	5.2721e-05	72.56	441.3	3.3470e-05	9.8947e-05	5.2723e-05	34.05	438.8

the variation of accuracy with different shape parameters and numbers of the supporting points. It can be seen that, using two layer nearest neighbor points, the accuracy of numerical solutions is improved. If there is only the first layer nearest neighbor points with small number of supporting points, the error is decreased with the increase of c, which is consistent with the conclusion in [36]. However, for large number of supporting points, with small shape parameter c, it is found that the accuracy changes sharply.

For a complex geometry, such as a multi connected domain, the present method is still very useful. For example, the computational domain is formed by two non concentric circles as shown in Fig. 5 . The centers of the external big circle and the internal small circle located at $(1, 1)$ with radius $r = 1$ and $(1.4, 1.1)$ with radius $r = 0.2$ respectively. In this example, we used 1354 points as shown in the left of Fig. 5 to simulate Equation (28) with variable order $\alpha(\mathbf{x}, t)$ on Dirichlet boundary condition. The errors obtained by the presented method is shown in the right of the Fig. 5 at $t = 1$. The magnitude of errors are very small.

5.2 Test problem with Neumann boundary condition

In order to validate the proposed method for the problem with Neumann boundary conditions, we firstly study the numerical results for Equation (28) with Neumann boundary over a unit circle. The computational grid is the same as the previous example as shown in Fig. 1. The approximate solutions at $t = 1$ with variable-order $\alpha(\mathbf{x}, t)$ and the absolute errors are plotted in Fig. 6. As one can see, the order of errors is acceptable and it shows the ability of the proposed method in solving such problems on non-regular domains with the Neumann boundary conditions.

A comparison between the numerical and exact solutions with different error norms at time $t = 1$ for two constant orders $\alpha = 0.5,\ 0.8$ and variable-order $\alpha(\mathbf{x}, t)$ is shown in Table 5 . It

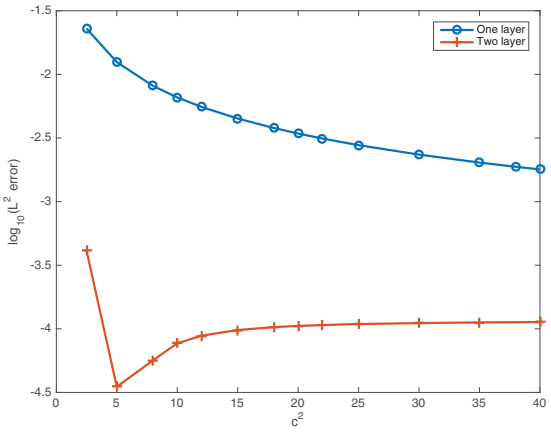

Figure 4: $\log_{10}$ (error) vs shape parameter c^2 with different supporting point distributions.

shows that the proposed method has good accuracy for the problem by employing the Neumann boundary conditions. Hence, it can be concluded that the proposed RBF-DQ method handles this kind of boundaries very well.

It should be noted that, In Fig. 1, the points are clustered on the boundary. In order to explore the impact of the point distribution, we present the results obtained by a new grid as shown in Fig. 7. The error indicates, although clustering points in the boundary can improve the accuracy, a common uniform grid is still very effective.

Table 5: L^2/L^∞ errors and RMS of errors obtained by local RBF-DQ method with Neumann boundary conditions

	Circular domain		
α	L^2	L^∞	RMS
0.5	8.2706e-04	1.5602e-03	1.3321e-03
0.8	1.5503e-03	2.7388e-03	2.4971e-03
$\alpha(\mathbf{x},t)$	1.8022e-03	3.3930e-03	2.9027e-03

In order to explore the grid convergence with the Neumann Boundary condition, we choose the same grids used for the analysis of the convergence for Dirichlet boundary condition and solve the same equation (28) with the variable order $\alpha(\mathbf{x},t)$. To reduce the influence of time discretization error, we take a smaller time step $\Delta t = 1/1000$. The numerical results of L^2, L^∞ and RMS errors are shown in Table 6. It can be seen that the error decreases as the number of grids increases. The condition numbers of the final solution matrices for the Neumann boundary condition are much larger than ones for the Dirichlet boundary condition. However, the matrix condition numbers decrease as the grid point numbers increase as shown in Table 6.

In order to show the effective of the present method for complicated problem, we also used the method to study Equation (28) with hybrid boundary conditions. The computational domain is formed by a pentagonal star and a 90 degrees circular arc (see Fig. 8). The point coordinates at

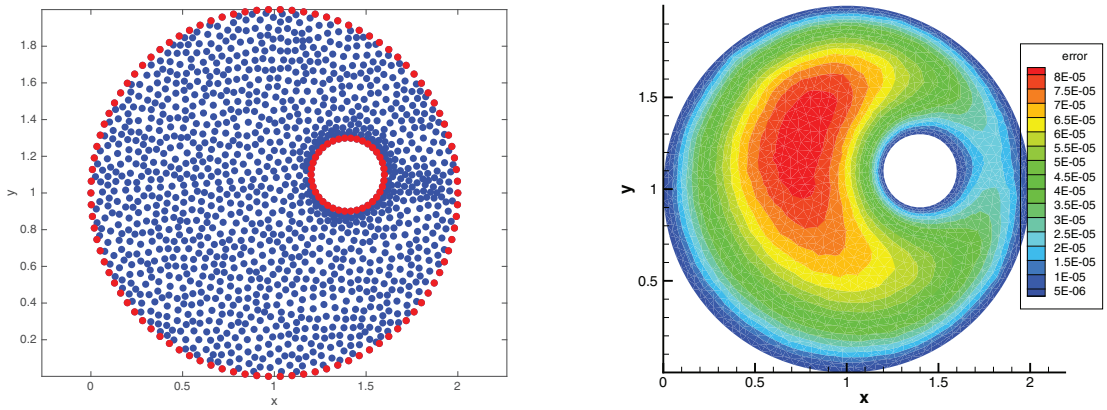

(a) Non-concentric circles and the points.

(b) The absolute error.

Figure 5: Points distribution and absolute error for Equation (28) with Dirichlet boundary condition on the computational domain.

Table 6: Grid convergence of local RBF-DQ method with Neumann boundary conditions ($\Delta t = 1/1000$).

N	L^2	L^∞	RMS	Cond.
214	3.0943e-03	6.3906e-03	4.8854e-03	4.1475e+03
421	1.9209e-03	4.2005e-03	3.0062e-03	2.3873e+03
873	8.4986e-04	2.1976e-03	1.3387e-03	2.0430e+03

the pentagonal star can be calculated by the following formula.

$$\begin{aligned} x_{2i-1} &= R\cos\tfrac{[90+72(i-1)]\pi}{180},\ y_{2i-1} = R\sin\tfrac{[90+72(i-1)]\pi}{180},\ i=1,\ldots,4 \\ x_{2i} &= r\cos\tfrac{[126+72(i-1)]\pi}{180},\ y_{2i} = r\sin\tfrac{[126+72(i-1)]\pi}{180},\ i=1,\ldots,3 \end{aligned} \tag{29}$$

where, $R = 2$ and $r = 1$. The Neumann boundary condition is enforced on the right of the shape labeled by "$\star$" and colored by red, and the Dirichlet boundary condition is enforced on the rest. For this special case, the total number of computational points is 1364 and the total cost of time is 227.85 seconds. The approximate solution and the absolute error are shown in Fig. 9. It can be seen that, although the boundaries with the Neumann boundary conditions include singular corner points, the final result looks still very fine.

We also consider the following variable fractional equation,

$$ {}_0^c D_t^{\alpha(\mathbf{x},t)} u(\mathbf{x},t) = (3+t^2)\Delta u(\mathbf{x},t) + f(\mathbf{x},t), \tag{30}$$

where

$$f(\mathbf{x},t) = \left[\frac{2}{\Gamma(3-\alpha)t^\alpha} - \frac{4(3+t^2)}{\beta}\left(-1+\frac{(x-0.05)^2+(y-0.05)^2}{\beta}\right)\right] t^2 e^{\frac{-(x-0.05)^2-(y-0.05)^2}{\beta}},$$

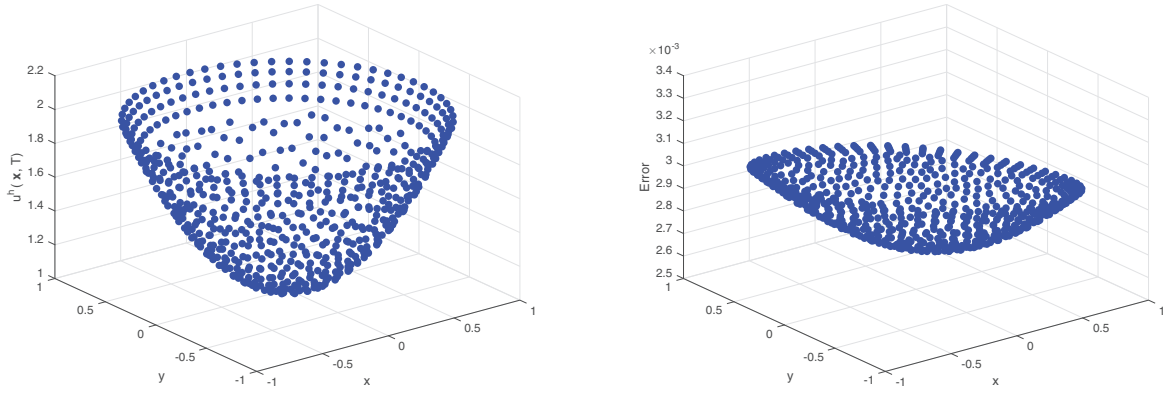

(a) The approximate solution.

(b) The absolute error.

Figure 6: The space graphs of the approximate solution and absolute error for Equation (28) with Neumann boundary condition on the circle domain ($N = 646$).

and

$$\alpha(\mathbf{x}, t) = 0.8 - 0.1\cos(xt)\sin(x) - 0.1\cos(yt)\sin(y),$$

with Neumann boundary condition. The exact solution is a Gauss pulse [30] as

$$u(\mathbf{x}, t) = t^2 e^{\frac{-(x-0.05)^2-(y-0.05)^2}{\beta}}.$$

Here, the irregular computational domain is obtained by the polar coordinate method [44], and is defined by

$$\rho = \frac{n+1}{n^2}(n + 1 - \cos n\theta),\ \theta \in [0, 2\pi].$$

The geometry for $n = 6$ and the grid points with total number 2125 points are shown in Fig. 10. The numerical solution and the error distributions for $\beta = 0.1$ are plotted in Fig. 11. The total cost of CPU time is 371.92 seconds. The results show that the method is applicable to various complex problems.

5.3 Variable-order fractional modeling of air pollution

The transport and diffusion of pollutants in the atmosphere is a challenging problem due to its physical complexity [50, 51]. An example of complexity is the description of diffusion under atmospheric turbulence. And Goulart et al think that the traditional differential equations do not adequately describe the problem of turbulent diffusion because usual derivatives are not well defined in the non-differentiable behavior introduced by turbulence [51]. The use of fractional calculus in modeling diffusion of pollutants is justified by the presence of anomalous diffusion due to turbulence. Hence Goulart et al set up some fractional derivative models for atmospheric dispersion of pollutants.

As a practical application, for Neumann boundary condition problem, we consider a variable-order fractional modeling of air pollution [10, 52]. In this study, the processes of transport and

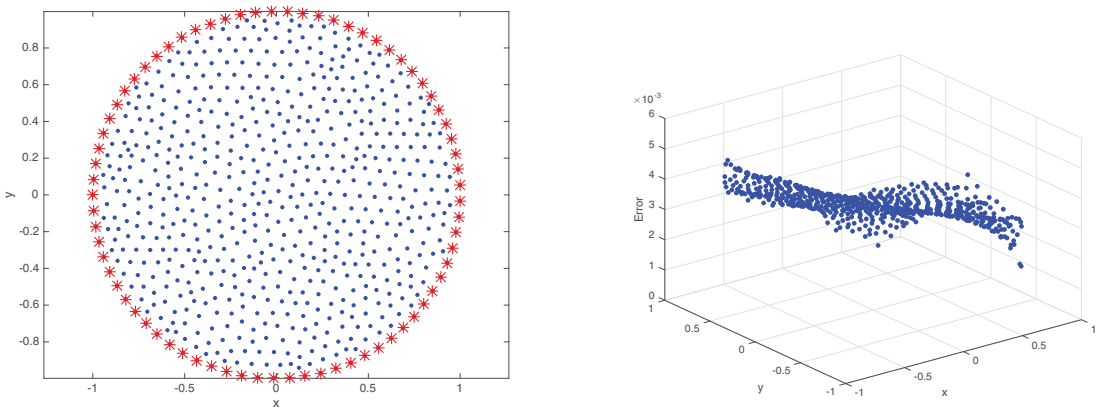

(a) The points. (b) The absolute error.

Figure 7: Points distribution and absolute error for Equation (28) with Neumann boundary condition on the computational domain ($N = 656$).

diffusion of pollutants in the atmosphere with obstacles are investigated. The equation represents a mass balance statement of pollutant materials when they are transported through the air, and is defined by

$$ {}_0^c D_t^{\alpha(\mathbf{x},t)} C(\mathbf{x},t) = \xi \Delta C(\mathbf{x},t) - \mathbf{v} \cdot \nabla C(\mathbf{x},t) + f(\mathbf{x},t), \tag{31} $$

where $C(\mathbf{x},t)$ is the concentration of pollutant materials, $\mathbf{v}$ is the wind velocity and ξ is the diffusion coefficient.

In the paper [10], the authors considered the air pollution with constant ξ and $\alpha(\mathbf{x},t) = 0.55 + 0.45\sin(xyt)$, but they only solved the problems with the homogeneous Dirichlet boundary conditions. However, the homogeneous Dirichlet boundary conditions are not realistic in the practical applications because the penetrability cannot be satisfied near the computational boundaries. So the method suggested in [10] is assumed that the air pollution does not touch the boundaries.

In order to reflect the real applications, based on our method, the homogeneous Neumann boundary condition on a complex domain from real world is considered as an example in this paper. There are several buildings in this domain (see the left of Fig. 12). In the paper [10], the constant wind velocity is considered, however, this is not real in the domain with the impact of the buildings. In order to get the wind velocity distributions, we firstly calculate the velocity distributions by an open source computational fluid dynamics (CFD) code SU2 developed by Stanford University [53]. For this special example, the fluid is incompressible and free-stream velocity is assumed to be $(1, 0.5)$. Then the wind velocity distribution in Equation (31) can be obtained. The calculated velocities distribution colored by the magnitude of velocity are demonstrated in the right of Fig. 12.

In the present study, a single source of pollutant with strength $f = 5$ is located in the domain of $2.5 \le x \le 2.7$ and $2.5 \le y \le 2.7$ and the diffusion coefficient is $\xi = 0.2$. The numerical solutions are presented with the integer-order $\alpha(\mathbf{x},t) = 1.0$ and the variable-order $\alpha(\mathbf{x},t) = 0.55 + 0.45\sin(xyt)$. The computational grid is shown in Fig. 12 and the time step is $\Delta t = 0.02$. The pollutant distributions at different time are shown in Figs. 13 and 14 by contour lines, and the values of the concentration of pollutant materials on different contour lines are labeled. These contour plots

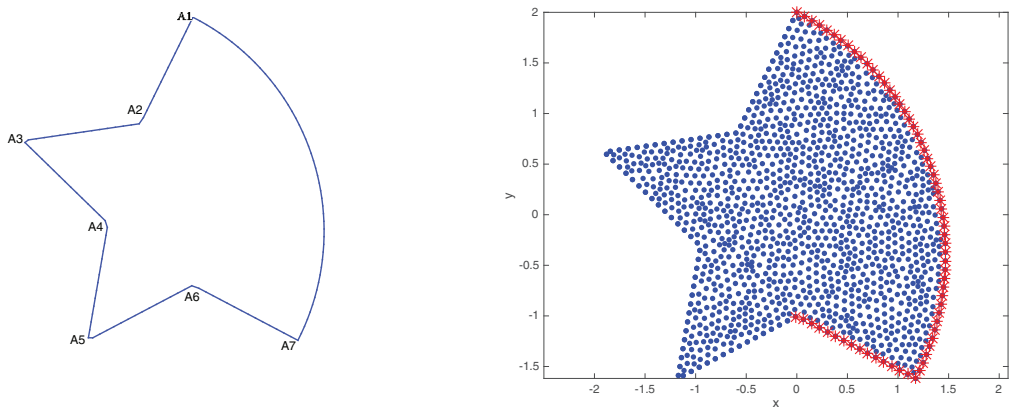

(a) Complex geometry. (b) Computational points.

Figure 8: Points distribution with hybrid Dirichlet and Neumann boundary condition on the computational domain (Neumann boundary condition labeled by red "$\star$").

show that the current method captures the pollutant feature throughout the computational domain. Furthermore, the numerical solutions with the integer-order equation are also presented. From these figures, we can conclude that, for this special problem, the concentration of pollutant materials of the present variable-order time model moves more slowly than that of the integer-order model. In particular, the field of concentration being positive is clearly evident in the numerical simulations. These results also show that the air pollution can successfully transfer across the boundaries. Hence, the current method can serve well for the problems with the Neumann boundary conditions.

6 Conclusion

In this paper, a local meshless RBF-based differential quadrature method was developed to simulate two-dimensional variable-order time fractional advection-diffusion equations. The proposed method was successfully applied on 2-D arbitrary domains of the numerical examples with Dirichlet and Neumann boundary conditions. The examples included constant-order and variable-order time fractional advection-diffusion equations. To examine the method suitable for the irregular domains, several complex geometries were tested and the robustness of the method to solve the irregular domains was presented. Furthermore, to test the ability of the proposed method for application problems, the numerical simulation for a variable-order fractional modeling off air pollution crossing several buildings was also investigated with the Neumann boundary conditions. The numerical results demonstrated that the present method can successfully deal with two-dimensional variable-order time fractional advection-diffusion equations on complex geometries with both the Dirichlet and the Neumann boundary conditions.

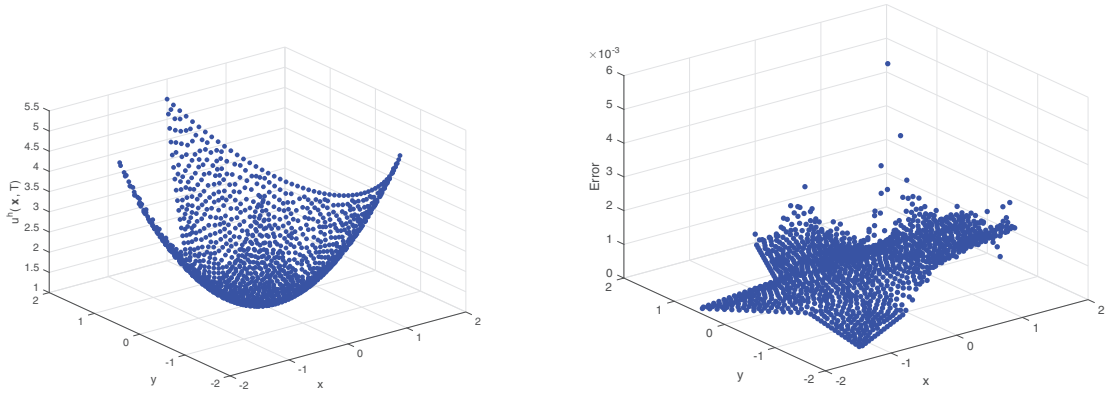

(a) The approximate solution.

(b) The absolute error.

Figure 9: The space graphs of the approximate solution and absolute error for Equation (28) with hybrid Dirichlet and Neumann boundary condition on the computational domain.

Acknowledgments

The authors thank the reviewers for the constructive and helpful comments on the revision of this article. Dr Jianming Liu was partially supported by the National Natural Science Foundation of China (Grant No. 91530325, 11102179), the Natural Science Foundation of the Jiangsu Higher Education Institutions of China (Grant No. 18KJA110001) and the Visiting Scholar Scholarship of the China Scholarship Council (Grant No. 201808320079). Dr Xiuling Hu was partially supported by the National Natural Science Foundation of China (Grant No. 11501262).

References

[1] V.V. Uchaikin. *Fractional Derivatives for Physicists and Engineers*. Higher Education Press, Beijing, 2013.

[2] W. Chen, H. Sun, and X. Li. *Fractional derivative modeling for mechanical and engineering problems*. Science Press, Beijing, 2010.

[3] F. Liu, P. Zhuang, and Q. Liu. *Numerical method of fractional partial differential equation and its application*. Science Press, Beijing, 2015.

[4] I. Podlubny. *Fractional differential equations*. Academic Press, San Diego, 1999.

[5] W. Chen and H. Sun. *Fractional differential equations and statistical models for anomalous diffusion*. Science Press, Beijing, 2017.

[6] C. F. Lorenzo and T.T. Hartley. Variable order and distributed order fractional operators. *Nonlinear Dynamics*, 29(1):57–98, 2002.

[7] L. Ramirez and C. Coimbra. On the variable order dynamics of the nonlinear wake caused by a sedimenting particle. *Physica D: Nonlinear Phenomena*, 240(13):1111 – 1118, 2011.

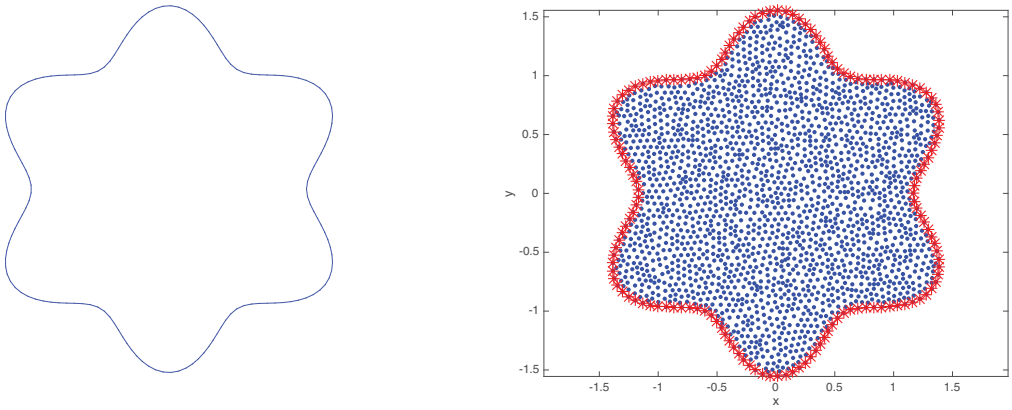

(a) Complex geometry.

(b) Computational points.

Figure 10: Complex geometry and points distribution.

[8] H. Sun, W. Chen, and Y. Chen. Variable-order fractional differential operators in anomalous diffusion modeling. *Physica A: Statistical Mechanics and its Applications*, 388(21):4586 – 4592, 2009.

[9] H.G. Sun, W. Chen, H. Wei, and Y.Q. Chen. A comparative study of constant-order and variable-order fractional models in characterizing memory property of systems. *The European Physical Journal Special Topics*, 193(1):185, 2011.

[10] A. Tayebi, Y. Shekari, and M.H. Heydari. A meshless method for solving two-dimensional variable-order time fractional advection diffusion equation. *Journal of Computational Physics*, 340:655–669, 2017.

[11] M.M. Meerschaert and C. Tadjeran. Finite difference approximations for fractional advection-dispersion flow equations. *Journal of Computational and Applied Mathematics*, 172(1):65 – 77, 2004.

[12] M. Dehghan. Weighted finite difference techniques for the one-dimensional advection–diffusion equation. *Applied Mathematics and Computation*, 147(2):307 – 319, 2004.

[13] S. Shen, F. Liu, J. Chen, I. Turner, and V. Anh. Numerical techniques for the variable order time fractional diffusion equation. *Applied Mathematics and Computation*, 218(22):10861 – 10870, 2012.

[14] A. Mohebbi, M. Abbaszadeh, and M. Dehghan. A high-order and unconditionally stable scheme for the modified anomalous fractional sub-diffusion equation with a nonlinear source term. *Journal of Computational Physics*, 240:36 – 48, 2013.

[15] M. Zayernouri and G.E. Karniadakis. Fractional spectral collocation methods for linear and nonlinear variable order FPDEs. *Journal of Computational Physics*, 293:312 – 338, 2015. Fractional PDEs.

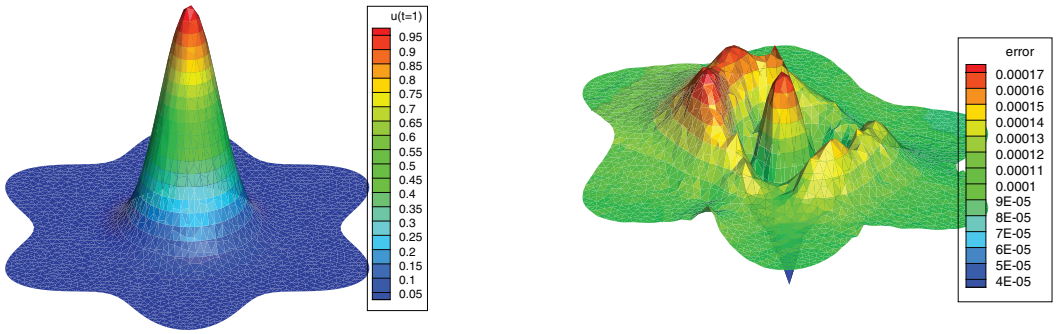

(a) The approximate solution.

(b) The absolute error.

Figure 11: The space graphs of the approximate solution and absolute error for Equation (30) with Neumann boundary condition on the computational domain.

[16] X. Zhao, Z.-Z. Sun, and G.E. Karniadakis. Second-order approximations for variable order fractional derivatives: Algorithms and applications. *Journal of Computational Physics*, 293:184 – 200, 2015.

[17] Y.M. Chen, Y.Q. Wei, D.Y. Liu, and H. Yu. Numerical solution for a class of nonlinear variable order fractional differential equations with legendre wavelets. *Applied Mathematics Letters*, 46:83 – 88, 2015.

[18] A. H. Bhrawy and M. A. Zaky. Numerical algorithm for the variable-order Caputo fractional functional differential equation. *Nonlinear Dynamics*, 85(3):1815–1823, Aug 2016.

[19] H. Ma and Y. Yang. Jacobi spectral collocation method for the time variable-order fractional mobile-immobile advection-dispersion solute transport model. *East Asian Journal on Applied Mathematics*, 6(3):337–352, 2016.

[20] R. Du, Z.P. Hao, and Z.Z. Sun. Lubich second-order methods for distributed-order time-fractional differential equations with smooth solutions. *East Asian Journal on Applied Mathematics*, 6(2):131–151, 2016.

[21] Z. Zhao and C. Li. Fractional difference/finite element approximations for the time-space fractional telegraph equation. *Applied Mathematics and Computation*, 219(6):2975 – 2988, 2012.

[22] B. Jin, R. Lazarov, Y. Liu, and Z. Zhou. The galerkin finite element method for a multi-term time-fractional diffusion equation. *Journal of Computational Physics*, 281:825 – 843, 2015.

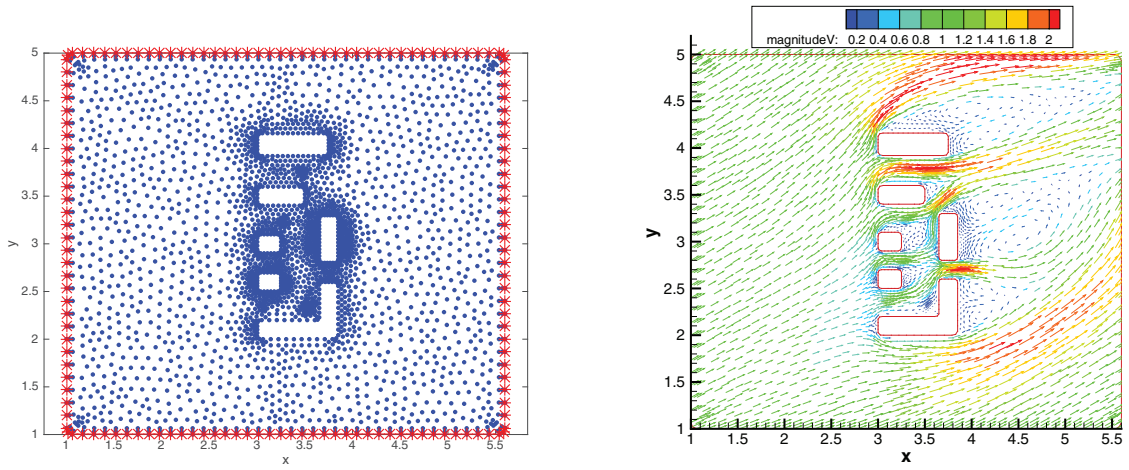

(a) Points distribution.

(b) Wind velocities distribution.

Figure 12: The computational grids for the domain with buildings and the wind velocity distribution for the model of air pollution.

[23] X. Zhao, X. Hu, W. Cai, and G.E. Karniadakis. Adaptive finite element method for fractional differential equations using hierarchical matrices. *Computer Methods in Applied Mechanics and Engineering*, 325:56 – 76, 2017.

[24] M. Dehghan, J. Manafian, and A. Saadatmandi. Solving nonlinear fractional partial differential equations using the homotopy analysis method. *Numerical Methods for Partial Differential Equations*, 26(2):448–479, 2009.

[25] S.L. Wu and T. Zhou. Parareal algorithms with local time-integrators for time fractional differential equations. *Journal of Computational Physics*, 358:135 – 149, 2018.

[26] X. Kin, M.K. Ng, and H. Sun. A separable preconditioner for time-space fractional caputo-riesz diffusion equations. *Numerical Mathematics: Theory, Methods and Applications*, 11(4):827–853, 2018.

[27] T.A. Biala and A. Khaliq. Parallel algorithms for nonlinear time–space fractional parabolic pdes. *Journal of Computational Physics*, 375:135 – 154, 2018.

[28] G.R. Liu and Y.T. Gu. *An Introduction to Meshfree Methods and Their Programming*. Springer Netherlands, 2005.

[29] Z.J.Fu, W. Chen, and L. Ling. Method of approximate particular solutions for constant- and variable-order fractional diffusion models. *Engineering Analysis with Boundary Elements*, 57:37 – 46, 2015. RBF Collocation Methods.

[30] M. Dehghan and M. Abbaszadeh. Element free galerkin approach based on the reproducing kernel particle method for solving 2d fractional tricomi-type equation with robin boundary condition. *Computers & Mathematics with Applications*, 73(6):1270 – 1285, 2017.

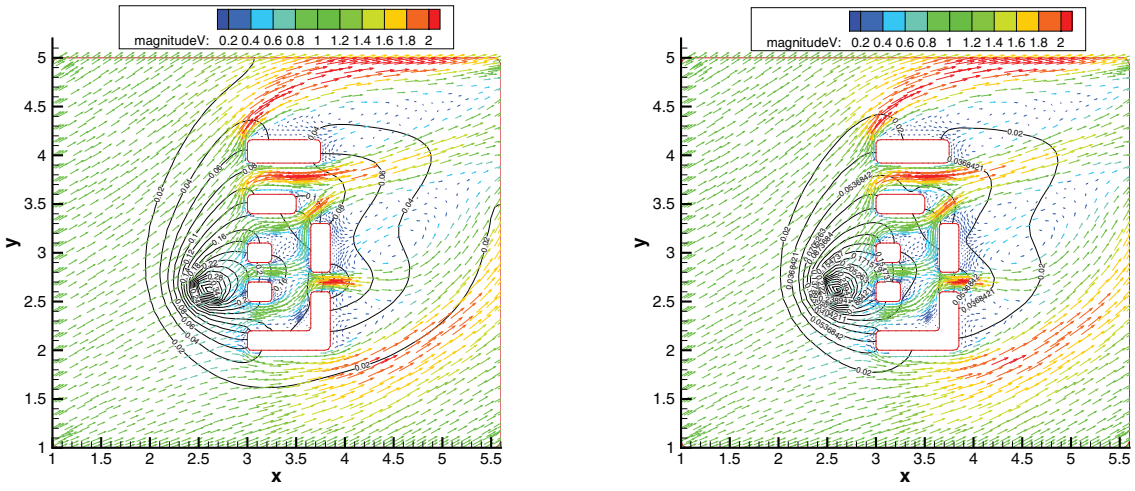

(a) $\alpha(\mathbf{x}, t) = 1.0$.

(b) $\alpha(\mathbf{x}, t) = 0.55 + 0.45\sin(xyt)$.

Figure 13: The pollutant distributions (time=4.0).

[31] P. Zhuang, Y.T. Gu, F. Liu, I. Turner, and P. Yarlagadda. Time-dependent fractional advection-diffusion equations by an implicit MLS meshless method. *International Journal for Numerical Methods in Engineering*, 88(13):1346–1362, 2011.

[32] A. Mardani, M.R. Hooshmandasl, M.H. Heydari, and C. Cattani. A meshless method for solving the time fractional advection-diffusion equation with variable coefficients. *Computers & Mathematics with Applications*, 75(1):122 – 133, 2018.

[33] G. Fasshauer. *Meshfree Approximation Methods with MATLAB*. World Scientific Publishers, Singapore, 2007.

[34] M. Dehghan and V. Mohammadi. The numerical solution of Cahn-Hilliard (CH) equation in one, two and three-dimensions via globally radial basis functions (GRBFs) and RBFs-differential quadrature (RBFs-DQ) methods. *Engineering Analysis with Boundary Elements*, 51:74 – 100, 2015.

[35] C. Shu. *Differential Quadrature and Its Application in Engineering*. Springer, London, 2000.

[36] C. Shu, H. Ding, and K.S. Yeo. Local radial basis function-based differential quadrature method and its application to solve two-dimensional incompressible Navier-Stokes equations. *Computer Methods in Applied Mechanics & Engineering*, 192(7):941–954, 2003.

[37] C. Shu, H. Ding, H.Q. Chen, and T.G. Wang. An upwind local RBF-DQ method for simulation of inviscid compressible flows. *Computer Methods in Applied Mechanics and Engineering*, 194(18):2001 – 2017, 2005.

[38] M.R. Hashemi and F. Hatam. Unsteady seepage analysis using local radial basis function-based differential quadrature method. *Applied Mathematical Modelling*, 35(10):4934 – 4950, 2011.

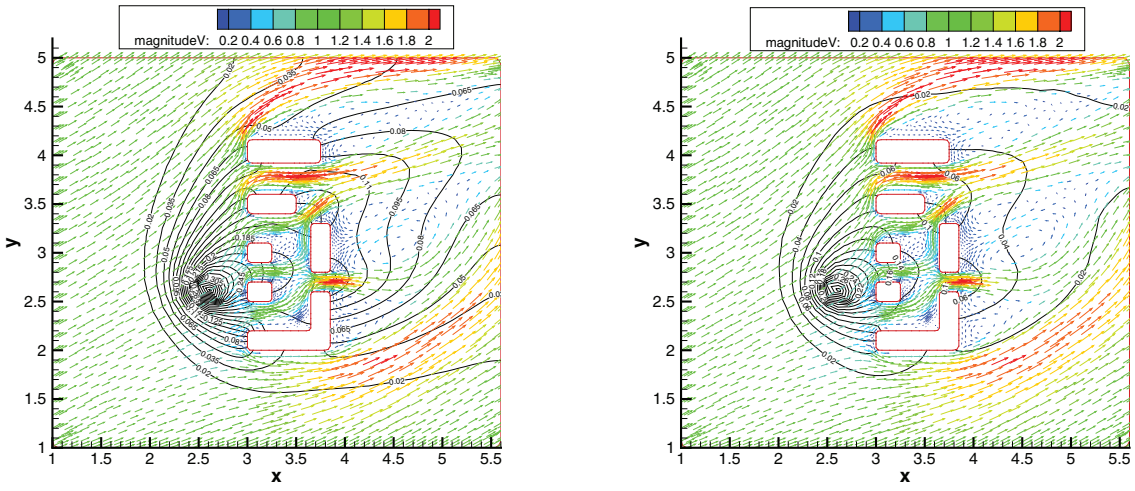

(a) $\alpha(\mathbf{x}, t) = 1.0$.

(b) $\alpha(\mathbf{x}, t) = 0.55 + 0.45\sin(xyt)$.

Figure 14: The pollutant distributions (time=8.0).

[39] M. Dehghan and A. Nikpour. Numerical solution of the system of second-order boundary value problems using the local radial basis functions based differential quadrature collocation method. *Applied Mathematical Modelling*, 37(18):8578 – 8599, 2013.

[40] Y.L. Chan, L.H. Shen, C.T. Wu, and D.L. Young. A novel upwind-based local radial basis function differential quadrature method for convection-dominated flows. *Computers & Fluids*, 89:157 – 166, 2014.

[41] A. Golbabai and A. Nikpour. Computing a numerical solution of two dimensional non-linear Schrödinger equation on complexly shaped domains by RBF based differential quadrature method. *Journal of Computational Physics*, 322:586 – 602, 2016.

[42] A. Golbabai and E. Mohebianfar. A new method for evaluating options based on multiquadric RBF-FD method. *Applied Mathematics and Computation*, 308:130 – 141, 2017.

[43] M. Dehghan and M. Abbaszadeh. Solution of multi-dimensional Klein–Gordon–Zakharov and Schrödinger /Gross–Pitaevskii equations via local Radial Basis Functions–Differential Quadrature (RBF–DQ) technique on non-rectangular computational domains. *Engineering Analysis with Boundary Elements*, 92:156 – 170, 2018.

[44] M. Hajiketabi and S. Abbasbandy. The combination of meshless method based on radial basis functions with a geometric numerical integration method for solving partial differential equations: Application to the heat equation. *Engineering Analysis with Boundary Elements*, 87:36 – 46, 2018.

[45] Y. Lin and C. Xu. Finite difference/spectral approximations for the time-fractional diffusion equation. *Journal of Computational Physics*, 225(2):1533 – 1552, 2007.

[46] Y.L. Wu and C. Shu. Development of RBF-DQ method for derivative approximation and its application to simulate natural convection in concentric annuli. *Computational Mechanics*, 29(6):477–485, 2002.

[47] R. Franke. Scattered data interpolation: Tests of some method. *Mathematics of Computation*, 38(157):181–200, 1982.

[48] J. Liu, N. Zhao, O. Hu, M. Goman, and X.K. Li. A new immersed boundary method for compressible Navier–Stokes equations. *International Journal of Computational Fluid Dynamics*, 27(3):151–163, 2013.

[49] L. Dinis, R.M. Natal Jorge, and J. Belinha. Analysis of 3D solids using the natural neighbour radial point interpolation method. *Computer Methods in Applied Mechanics and Engineering*, 196(13):2009 – 2028, 2007.

[50] C.W. Tessum, J.D. Hill, and J.D. Marshall. InMAP: A model for air pollution interventions. *PLOS ONE*, 12(4):1–26, 2017.

[51] A.G.O. Goulart, M.J. Lazo, J.M.S. Suarez, and D.M. Moreira. Fractional derivative models for atmospheric dispersion of pollutants. *Physica A: Statistical Mechanics and its Applications*, 477:9 – 19, 2017.

[52] E. Runca, P. Melli, and F. Sardei. An analysis of a finite-difference and a Galerkin technique applied to the simulation of advection and diffusion of air pollutants from a line source. *Journal of Computational Physics*, 59(1):152 – 166, 1985.

[53] T.D. Economon, F. Palacios, S.R. Copeland, T.W. Lukaczyk, and J.J. Alonso. SU2: An open-source suite for multiphysics simulation and design. *AIAA Journal*, 54(3):828–846, 2016.